Report - Part 3

Seismic Analysis of High Voltage Power Line Truss

June 23, 2025

[1]:
```
import numpy as np
import matplotlib.pyplot as plt
import os
from matplotlib import gridspec
from mpl_toolkits.axes_grid1 import make_axes_locatable
import matplotlib.pyplot as plt
import scipy.io as sio
from scipy.io import loadmat
import random
import pandas as pd
```

[2]:
```
# Defining parameters

student_number = 5381827
student_number = list(str(student_number))
for i in range(len(student_number)):
    student_number[i] = int(student_number[i])
A, B, C, D, E, F, G = student_number


g = 9.81                    # Gravitational acceleration [m/s^2]
xi = 0.040 + C * 1e-3       # Damping ratio []
PGA = (0.33 + D * 1e-2)     # Peak ground acceleration [g]
gamma = 1.4                 # Importance factor [] - Importance class IV␣
↪(assigned) corresponds to gamma=1.4 according to EN1998-1-1 (par 4.2.5)
a_g_ref = PGA*gamma         # Horizontal Reference acceleration [g] - Type 2␣
↪Earthquake (M_s = 5.0, assigned parameter)
a_vg_ref = a_g_ref*0.45     # Vertical Reference acceleration [g] - Type 2␣
↪Earthquake (M_s = 5.0, assigned parameter)

print(f"Damping ratio: {xi:.3}")
print(f"Peak Ground Acceleration (excluding importance factor): {PGA*g} m/s^2")
print(f"Horizontal Reference Acceleration for EN1998-1: {a_g_ref*g} m/s^2")
print(f"Vertical Reference Acceleration for EN1998-1: {a_vg_ref*g} m/s^2")
```

```
Damping ratio: 0.048
```

```
Peak Ground Acceleration (excluding importance factor): 3.3354000000000004 m/s^2
Horizontal Reference Acceleration for EN1998-1: 4.66956 m/s^2
Vertical Reference Acceleration for EN1998-1: 2.101302 m/s^2
```

1 Section 3.a

The pushover method of analysis is based on the imposition of a displacement pattern based either on uniform or modal deformed state. The standard operational procedure given by Eurocode 1998-1 begins with the derivation of the elastic spectrum based on a limited number of parameters that aim at predicting both Earthquake excitation and soil behavior. The first potential inconsistency when dealing with the Groningen seismic activity is that vertical accelerations are dominant in artificially induced Earthquakes, whereas the code assumes lateral excitations to be the critical design case (as can be seen in the coefficient table at 3.2.2.3 of EN1998-1). This particular feature is also relevant for the appropriate choice of mode to be used in the application of the modal displacement pattern. The pushover method relies on the ability of the single selected mode to describe the structural response to the excitation. In the case of the structure of interest the most critical loading condition is expected to be caused by lateral excitations, well represented by mode 1 and 2. These modes are however not able to represent properly the vertical component which is expected to be dominant in an Earthquake from the Groningen region. More generally, such considerations are especially crucial for structures whose stiffness relies on self-weight (i.e. a masonry structure with a disconnected roof). Another feature that may be relevant depending on the structure under analysis is that artificially induced earthquakes are characterized by high-energy release at higher frequencies, which may be a determining factor for the appropriate selection of modal pattern and is particularly important for short-period structures.

2 Section 3.b

2.1 Capacity vs Demand- Iterative procedure

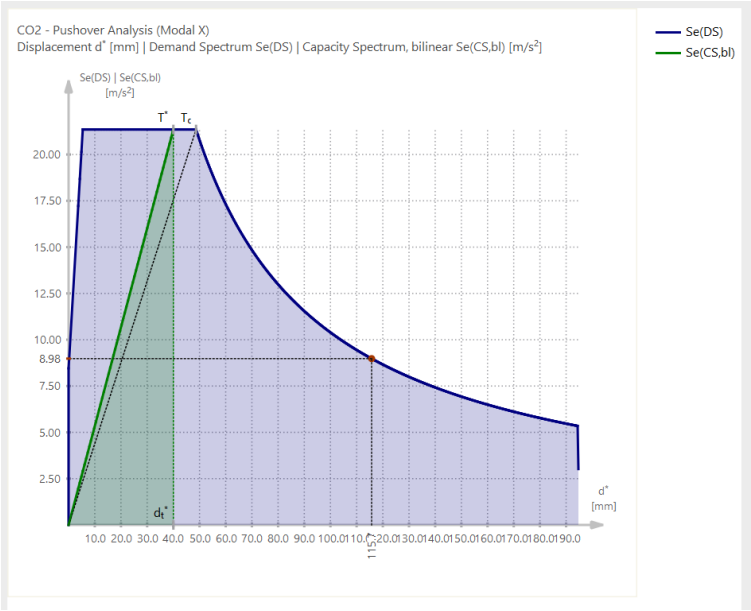

Original Reference PGA $a_{g,R} = 3.34m/s^2$

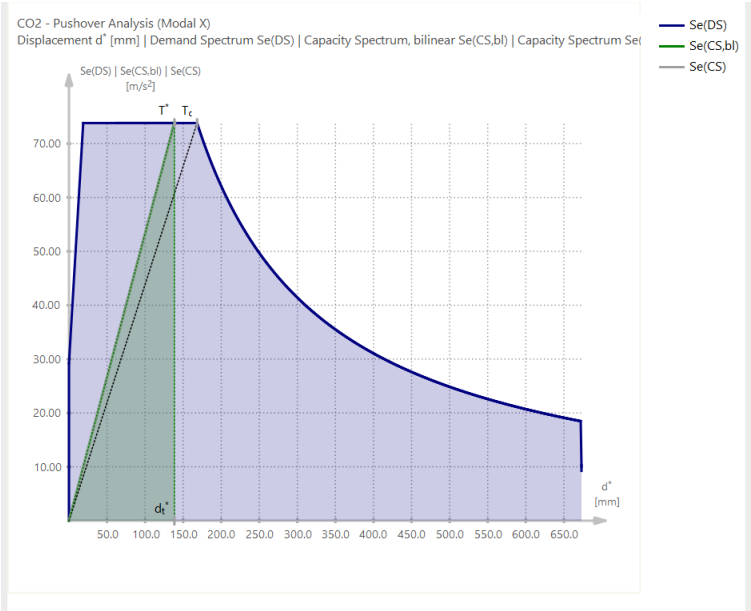

Increased Reference PGA $a_{g,R} = 10.00m/s^2$

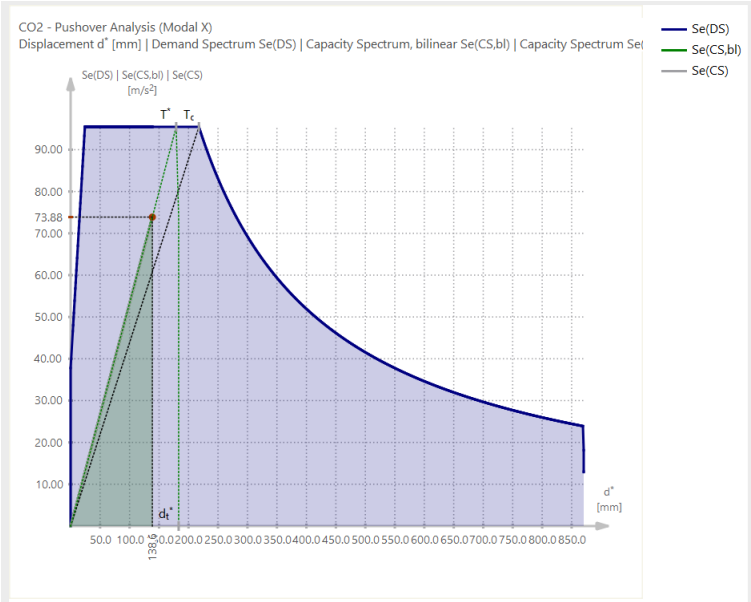

Increased Reference PGA $a_{g,R} = 15.00m/s^2$

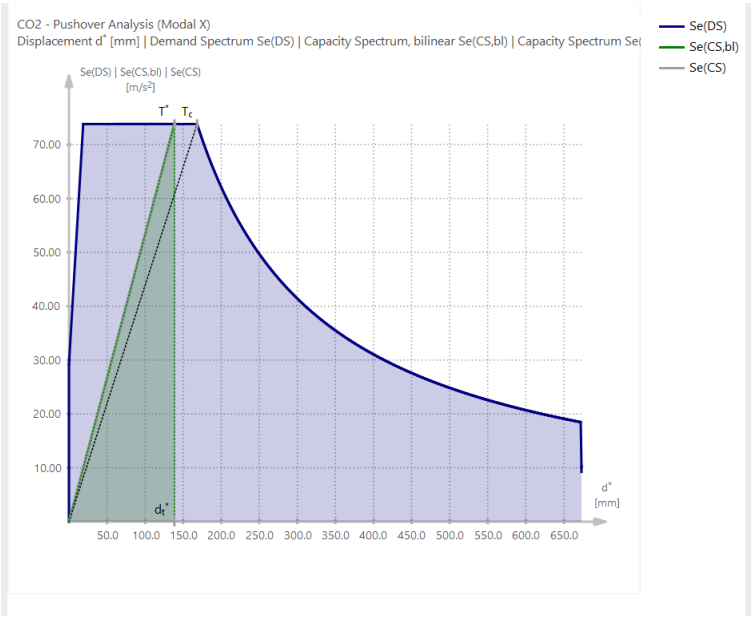

Increased Reference PGA $a_{g,R} = 11.60m/s^2$, limit state

Our structure is able to withstand the acceleration imposed by EN1998-1 standard within its elastic regime. According to the simulation no plastic response is developed within failure.So different iterations were done by adjusting the seismic demand to higher values by adjusting the PGA. Upon further research, the conclusion that a more refined model would be necessary in order to develop a plastic phase in the capacity spectrum was reached. I would in fact be necessary to include a model of the connections in order to correctly reproduce structural collapse, whereas the current model can deform indefinitely. This was the interpretation given to the following diagram, where Von Mises equivalent stresses are plotted.

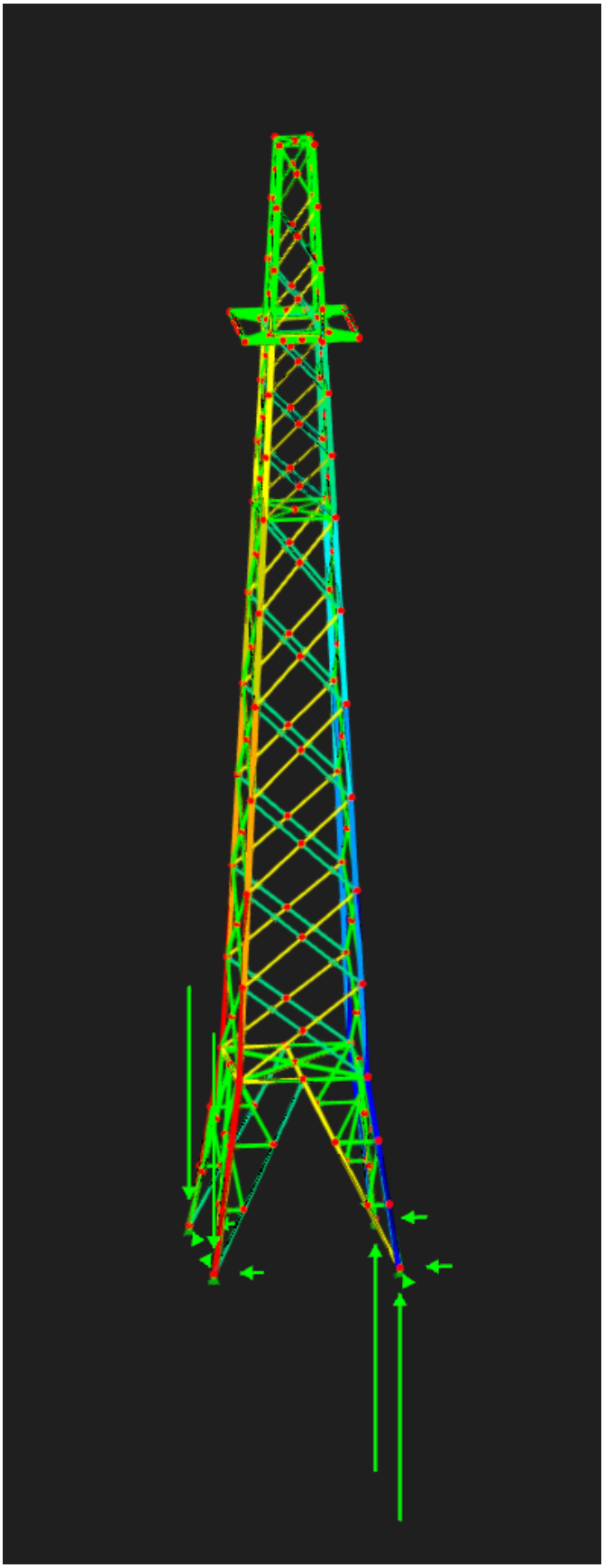

3 Section 3.c

According to EN1998-1-2005 section 4.3.3.2.1 a single mode approximation is a viable option when the period of the chosen mode of vibration satisfies the following conditions:

$$T_n < \begin{cases} 4 * T_C \\ 2s \end{cases}$$

In our design scenario $T_C = 0.3s$ and $4{*}T_C = 1.2s$. Mode 2 was chosen for the analysis in X direction and respects the above mentioned condition with $T_2 = 0.27s$. Mode 1 was chosen for the analysis in Y direction with $T_1 = 0.27s$. No further load combinations are therefore deemed necessary. On a more qualitative level, Mode 1 and 2 present a modal shape that maximize displacement at the top of the structure in the main directions. The corresponding load patterns are considered an appropriate choice in maximizing the overturning moment, which is expected to be the most critical action for a cantilever beam structure. Finally, the relatively high Effective Modal Mass Factor of Mode 1 and 2 set at 0.44 (see table in Section 5 Part A) supports such decision, especially since a single modal shape needs to be selected in this analysis.

3.1 Section 4 - Time History Analysis

A Time History Analysis was carried out as part of the seismic assessment of the structure. Signal 1 was chosen from previously processed data and the model was subjected to the derived accelerations in the three principal directions.
As part of this analysis a limitation of the RFEM software was encountered: the Stress-Analysis module did not support nonlinear material behavior for members. As a consequence the analysis was carried out in both bilinear and linear regimes, but stresses were computed for linear regime. It is therefore implicitly assumed that the linear behavior of the structure is sufficient to identify critical stresses location.

The comparison of **maximum displacements** yielded the following results:

DOF	Member	Material Bilinear	Material Linear	Description
X	313	-83.5 mm	-83.3 mm	Top of the tower
Y	365	87.0 mm	86.3 mm	Antenna on mounting bracket
Z	329	-19.3 mm	17.9 mm	Horizontal Bracing (2nd order)
ϕ_x	365	41.7 mrad	41.0 mrad	Antenna on mounting bracket
ϕ_y	329	-18.4 mrad	17.5 mrad	Horizontal Bracing (2nd order)
ϕ_z	119	-70.3 mrad	-70.6 mrad	Strut in basal truss (lowest)

High-stress locations (most relevant):

Member No.	Location x [m]	Stress Existing [N/mm2]	Stress Limit [N/mm2]	Stress Ratio η [-]
111	1.874	200.340	235.000	0.853
117	0.000	201.047	235.000	0.856
311	1.707	211.905	235.000	0.902
312	0.000	215.914	235.000	0.919
329	0.000	258.318	235.000	1.099
331	1.354	258.399	235.000	1.100

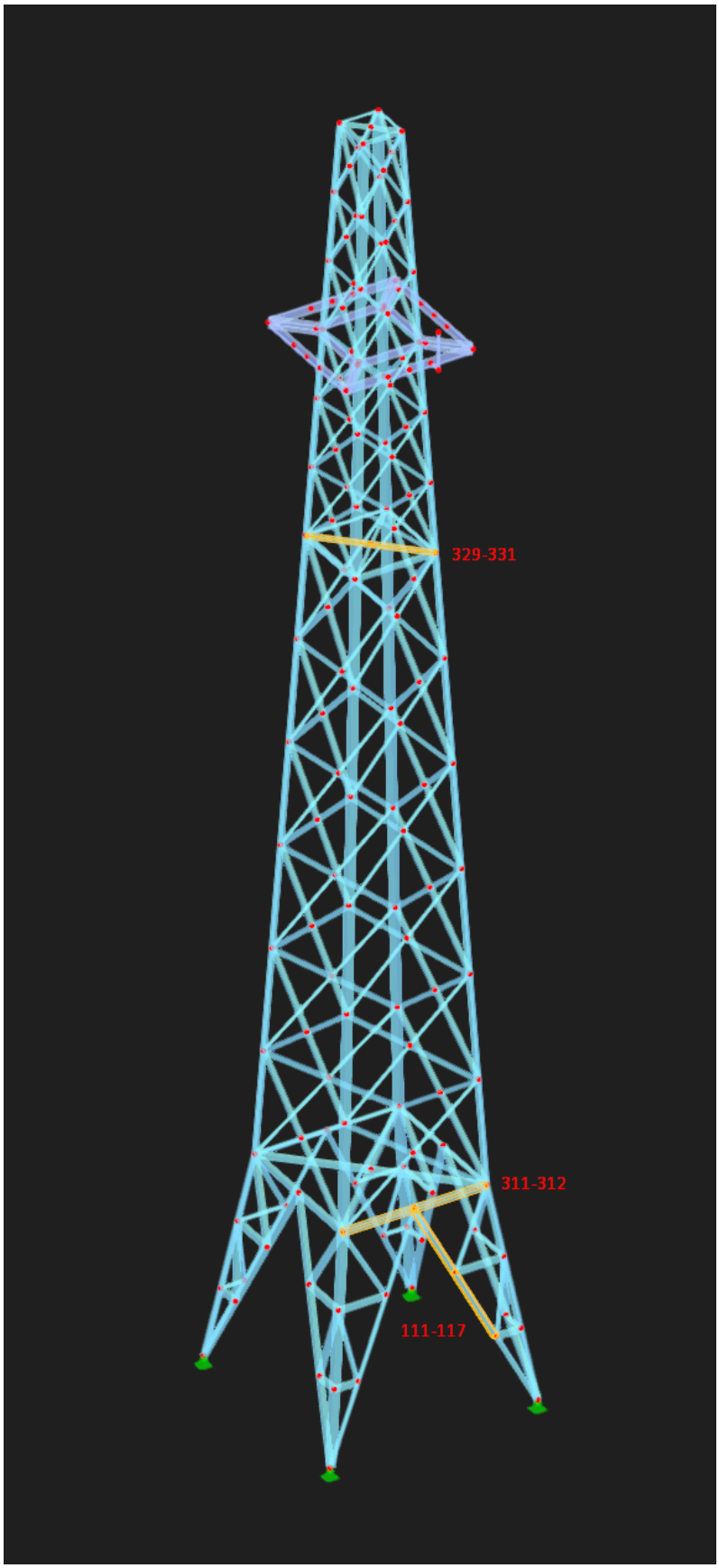
329-331
311-312
111-117

Displayed stresses were computed with Von Mises equivalent stresses criterion. Comparing stresses with yielding stress values for the chosen material shows that most critical excitation is located at the interface between Members 329-331. At such locations the computed stresses due to the ground acceleration provided by the timeseries (Signal 1) input in the model exceed the limit stress of the material causing failure of the structure. This finding is consistent with Spectral and Modal analysis results. Mode 41, which excites precisely members 329-331 as shown in the following figure, has in fact a period of $0.065s$ which closely matches the peak frequency of the vertical component of the Elastic Response Spectrum computed for the chosen signal.

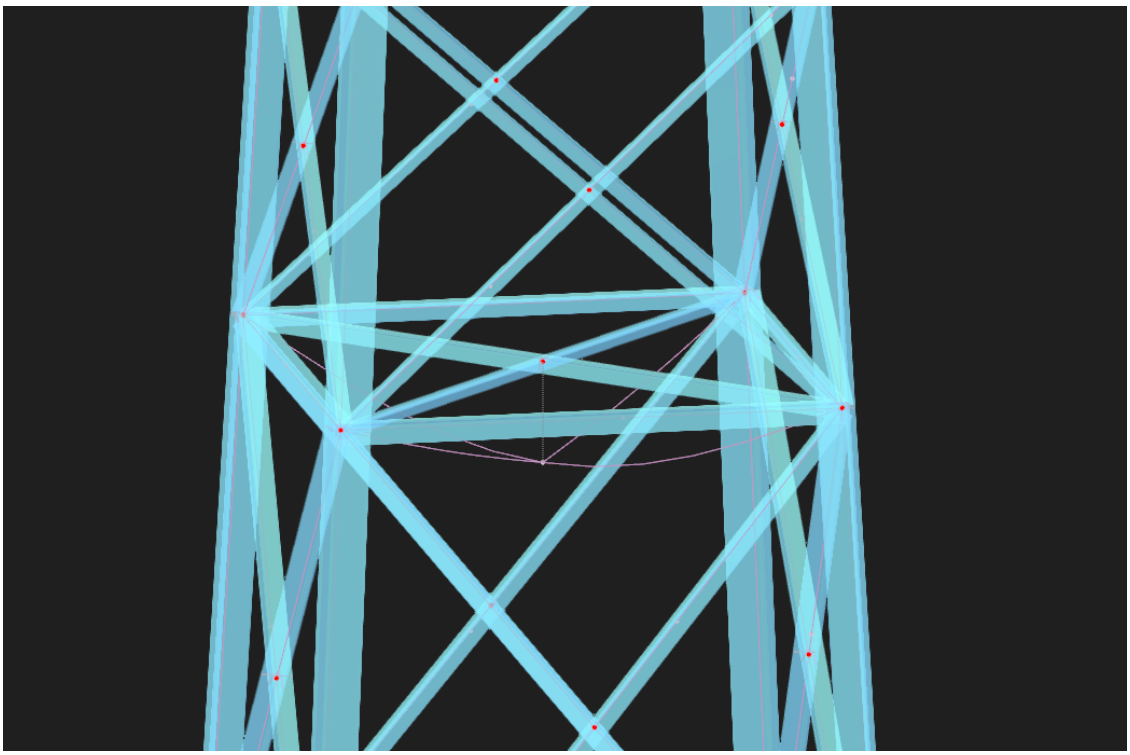

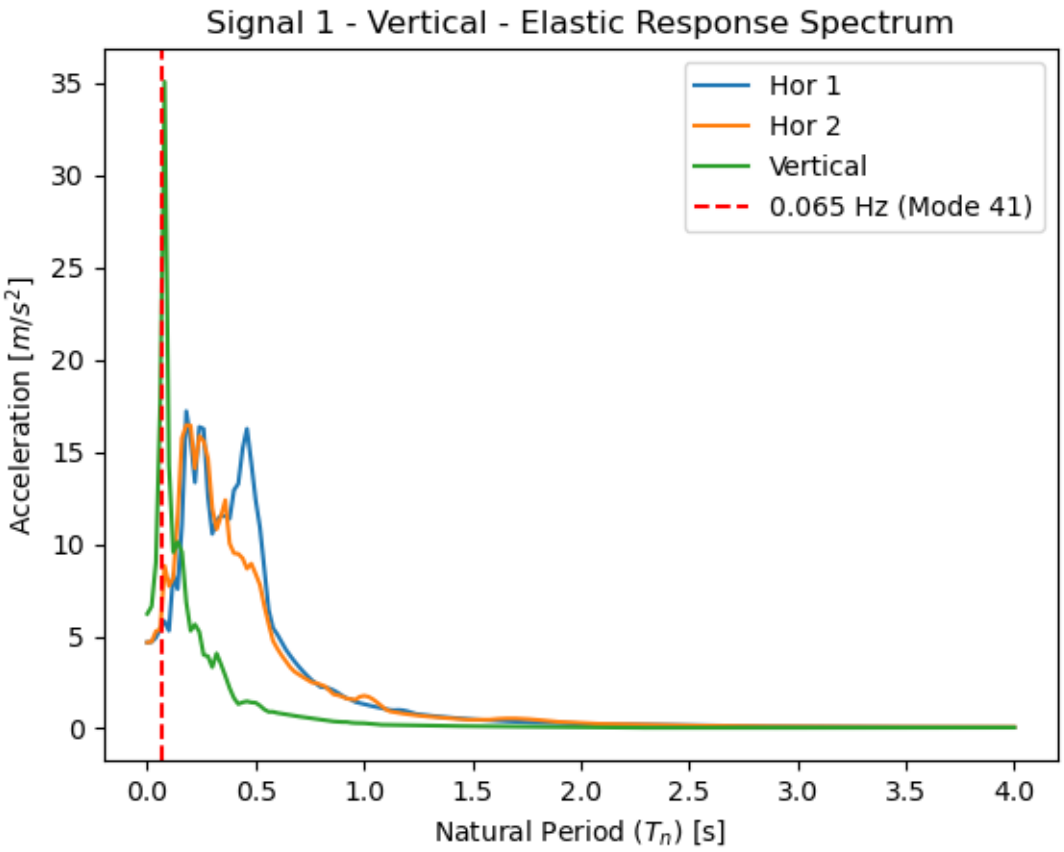

In conclusion, the results of the Time Series Analyisis would hint towards a vulnerability of the structure to vertical accelerations and therefore inadequacy of the design to withstand seismic load. It is however worth pointing out that the peak stress observed in members 329-331 is the result of a resonance between the spectral component located at 15.38 Hz in Signal 1 and mode 41 of the structure. Given that Signal 1 shows an unusually high peak when compared to the other signals that were taken into consideration, this result may require further examination of the validity and/or statistical relevance of Signal 1 and the design may not need further refinement. If the signal were to be considered relevant, the possible options to mitigate the problem would include the use of stronger profiles for members 329-331 and/or damping devices that would target displacements at the intersection of member 329-331. In both cases the analysis should be repeated as both options may in principle affect the dynamic behavior of the structure, potentially relocating the critical section.

4 Section 5 - Response Spectrum Analysis

4.1 Part A

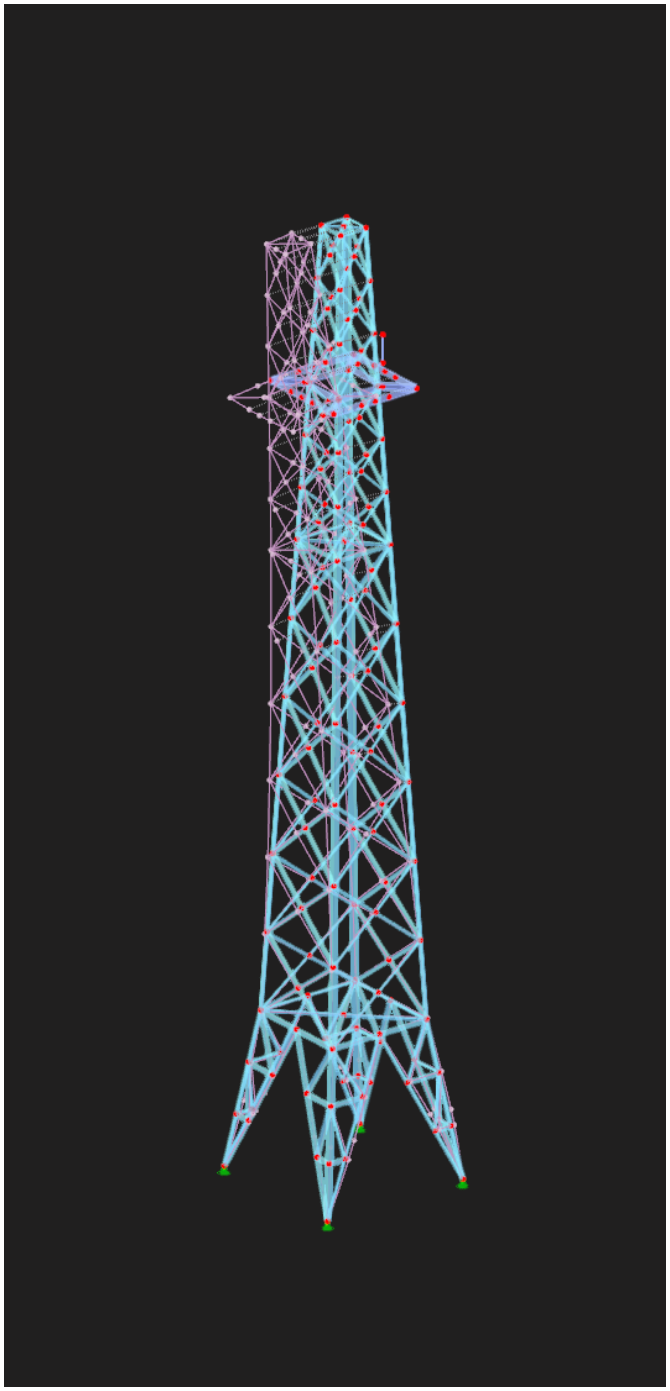

Modal shape 1

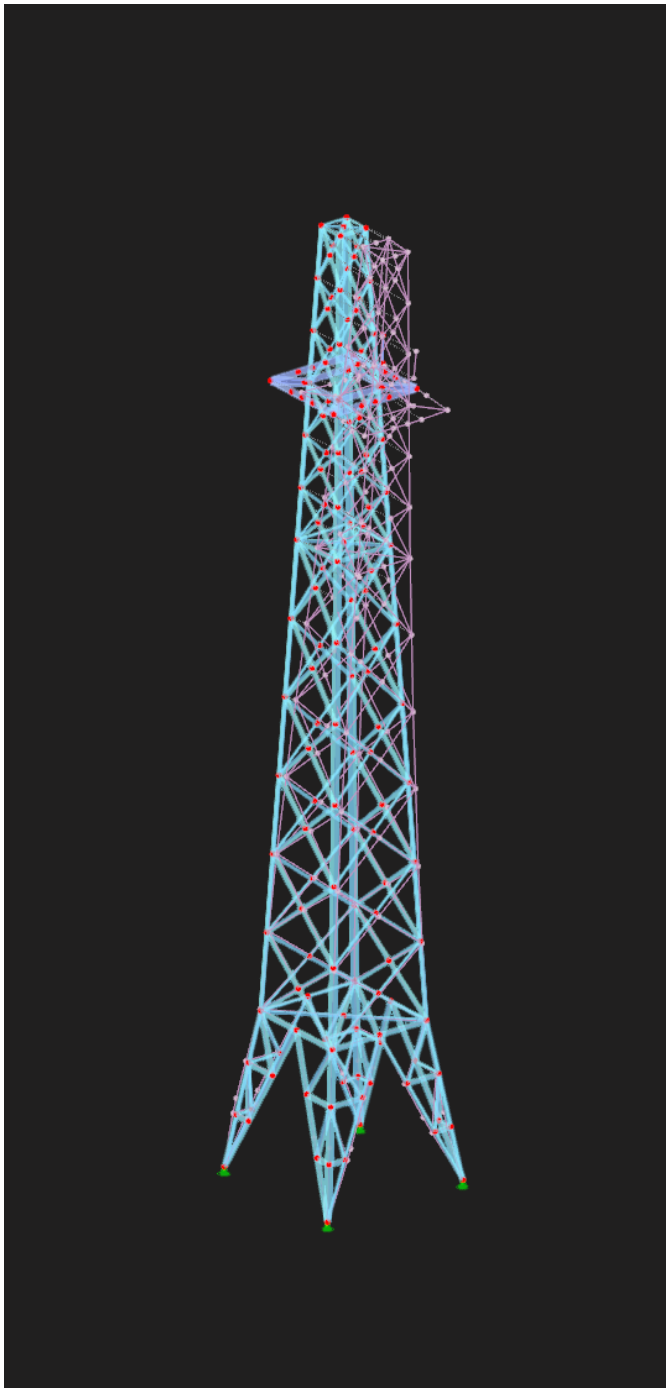

Modal shape 2

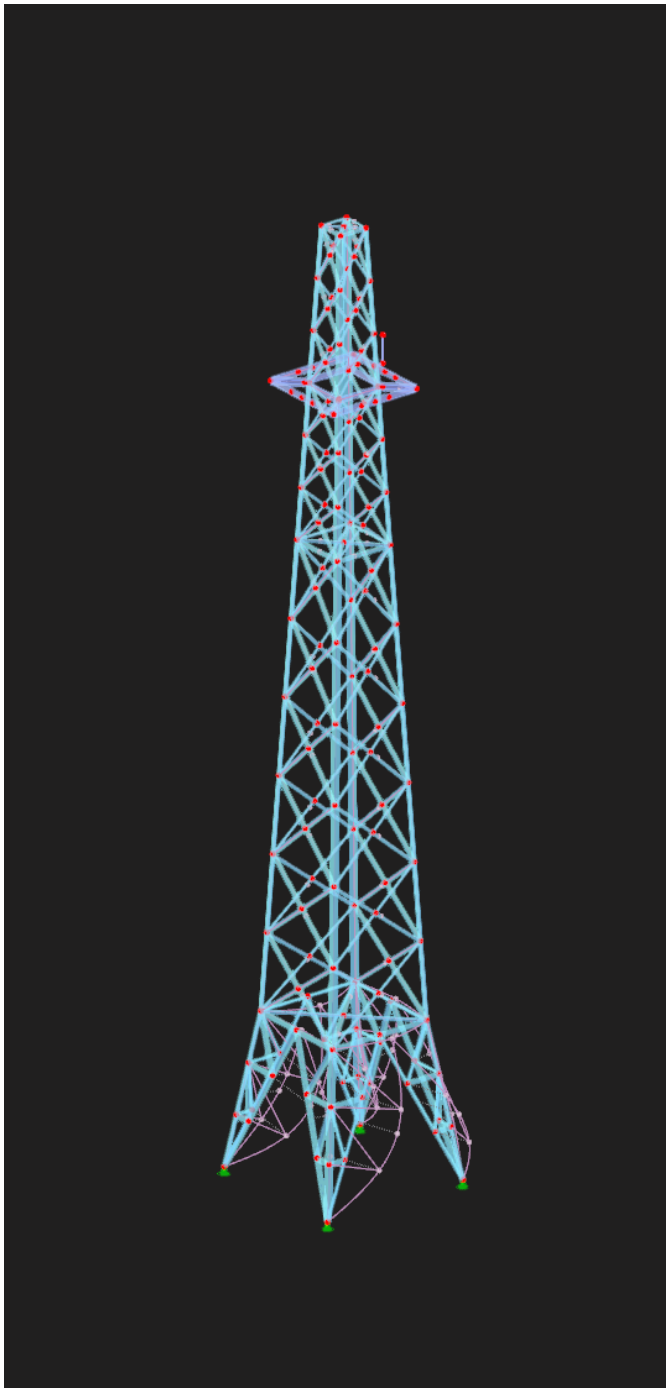

Modal shape 3

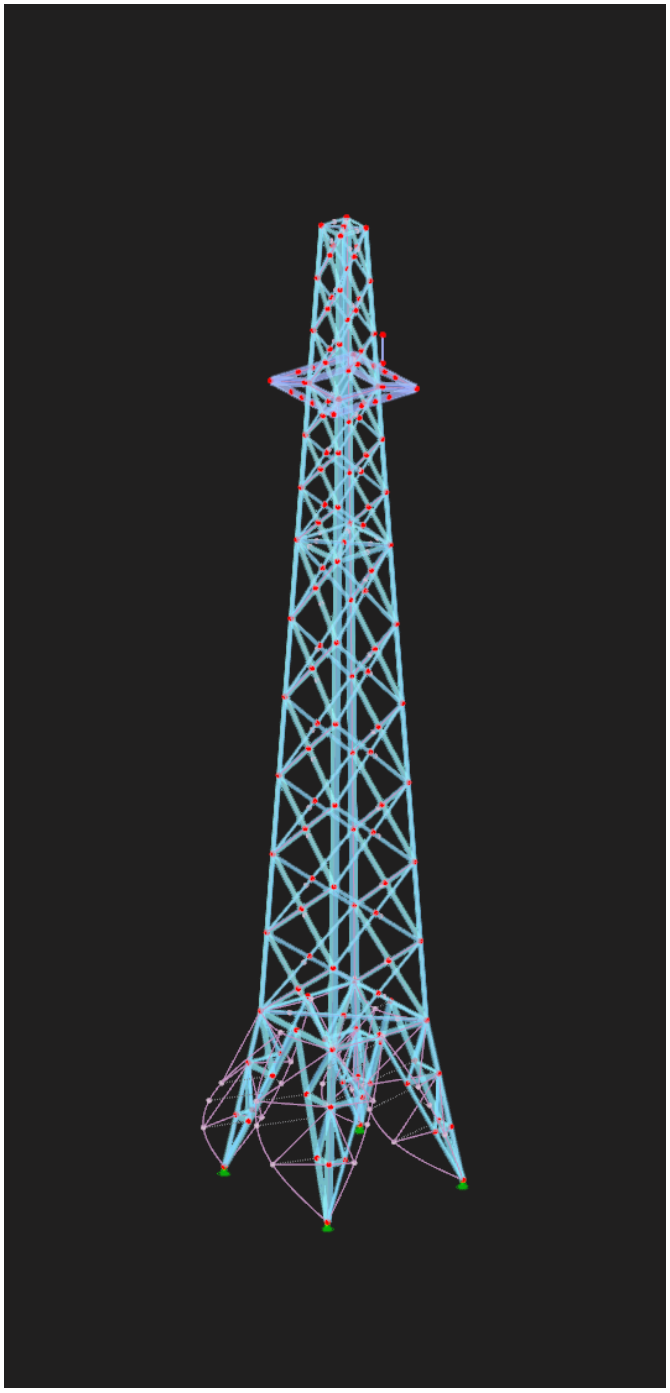

Modal shape 4

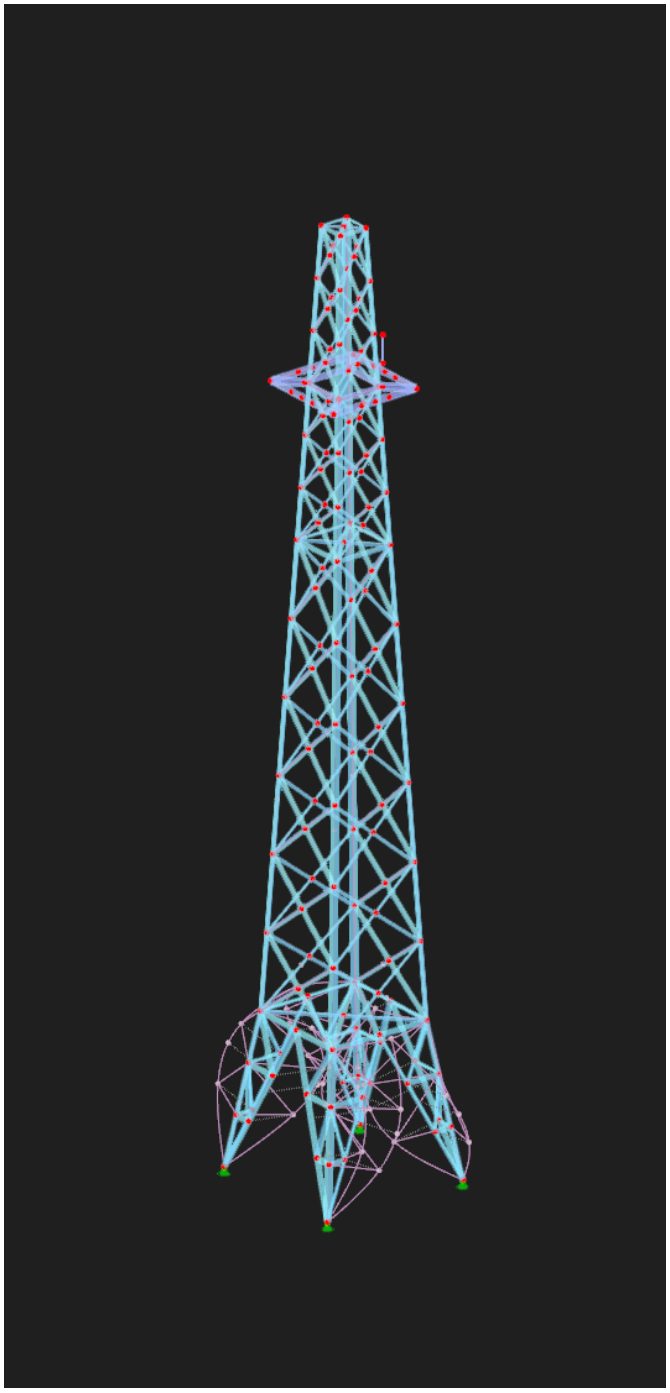

Modal shape 5

Mode Nr	NF	Modal Mass	EMM X	EMM Y	EMM Z	EMM ϕ_x	EMM ϕ_y	EMM ϕ_z
1	3.667	1683.0	89.4	3848.9	0.0	364106.00	7104.35	0.00
2	3.668	1682.2	3849.0	89.4	0.0	7102.31	364118.00	0.01
3	5.839	449.9	428.6	217.7	0.0	28487.50	41881.80	0.00
4	5.839	450.0	217.7	428.5	0.0	41887.40	28488.40	0.00
5	5.855	544.5	0.0	0.0	0.0	0.00	0.00	0.00
28	12.026	0	0	0	0.4	0.16	10369	0
55	18.897	0	0.5	0.4	18.92	0.03	10792.4	0
84	25.518	0.2	0	3684.2	0.61	16.97	13.18	0

Mode Nr	NF	Factor X	Factor Y	Factor Z	Factor ϕ_X	Factor ϕ_Y	Factor ϕ_Z
1	3.667	0.010	0.440	0.000	0.510	0.010	0.000
2	3.668	0.440	0.010	0.000	0.010	0.510	0.000
3	5.839	0.049	0.025	0.000	0.040	0.059	0.000
4	5.839	0.025	0.049	0.000	0.059	0.040	0.000
5	5.855	0.000	0.000	0.000	0.000	0.000	0.000
28	12.026	0	0	0	0	0	0.335
55	18.897	0	0	0	0	0	0.349
84	25.518	0	0.421	0	0	0	0

Inspecting the results of the modal analysis for 500 modes, the most relevant modes are mode 1 and 2 with a modal mass factor of 0.44 in for translational y and x direction respectively. These modes are also relevant to describe the global bending behavior of the truss structure with a modal mass factor of 0.51 in rotational x-direction and y-direction respectively. The similarity in properties between the two modes is to be expected as a result of the highly symmetric geometry of the structure. Mode 3 and 4 concern deformations of the basal supports of the truss, however their contribution is secondarily relevant to describe the dynamic behavior of the structure and may be arguably excluded from the analysis. In fact, EN1998-1 recommends a threshold of 0.05 for the participation ratio in the selection of modes as part of the truncation process, however 0.049 is hereby regarded as a relatively high contribution for a single mode. Mode 5 is interpreted as a numerical artifact and therefore irrelevant. The first 5 modes are highly inadequate to describe the deformation of the structure in vertical and torsional directions (translation and rotation about z). The most relevant mode for the former direction would be mode 84 (with a mass participation ratio (z) of 0.421) while modes 28 and 55 are the main contributors for the latter direction (counter-clockwise and clockwise torsion) with mass participation ratio of 0.339 and 0.349 respectively.

4.2 Part B

As mentioned in relation to Time History Analysis, due to RFEM features, maximum displacements were computed for both linear and nonlinear material, while stress-analysis was carried out for linear material only.

CQC method was preferred to the SRSS rule to combine structural modes. This choice was based on the robustness of CQC when dealing with modes of vibration close in frequency. Although the case

at hand did not specifically require such attention CQC was the preferred choice as more reliable and advanced modelling option. Moreover a damping ratio of 5% was taken as a realistic assumption for all modes, setting the domain within the range of applicability of the CQC method. Given the EN1998-1 spectra wide band range CQC was also deemed more appropriate to the specific design situation. SRSS was in turn selected to combined different directional seismic components. This method was preferred to the absolute sum method, which was deemed over-conservative, and to the scaled sum method, which was discarded for its questionable approach to modelling the real physical relation among seismic components from different directions.

DOF	Member	Material Bilinear	Material Linear	Description
X	321	61.3 mm	61.3 mm	Top of tower
Y	309	61.3 mm	61.3 mm	Top of tower
Z	333	11.5 mm	11.5 mm	Horizontal Bracing (1st order)
ϕ_x	239	12.0 mrad	12.0 mrad	Strut in basal truss (2nd from bottom)
ϕ_y	177	12.0 mrad	12.0 mrad	Strut in basal truss (2nd from bottom)
ϕ_z	181	36.5 mrad	36.5 mrad	Strut in basal truss (lowest)

High-stress locations (most relevant):

Member No.	Location x [m]	Stress Existing [N/mm2]	Stress Limit [N/mm2]	Stress Ratio η [-]
81	1.183	117.558	235.000	0.500
84	0.000	119.666	235.000	0.509
143	1.183	117.466	235.000	0.500
146	0.000	119.577	235.000	0.509
205	1.183	117.314	235.000	0.499
208	0.000	119.421	235.000	0.508
267	1.183	117.533	235.000	0.500
270	0.000	119.641	235.000	0.509
311	1.707	126.505	235.000	0.538
312	0.000	126.471	235.000	0.538
315	1.707	126.560	235.000	0.539
316	0.000	126.524	235.000	0.538
319	1.707	126.516	235.000	0.538
320	0.000	126.471	235.000	0.538
323	1.707	126.512	235.000	0.538
324	0.000	126.444	235.000	0.538

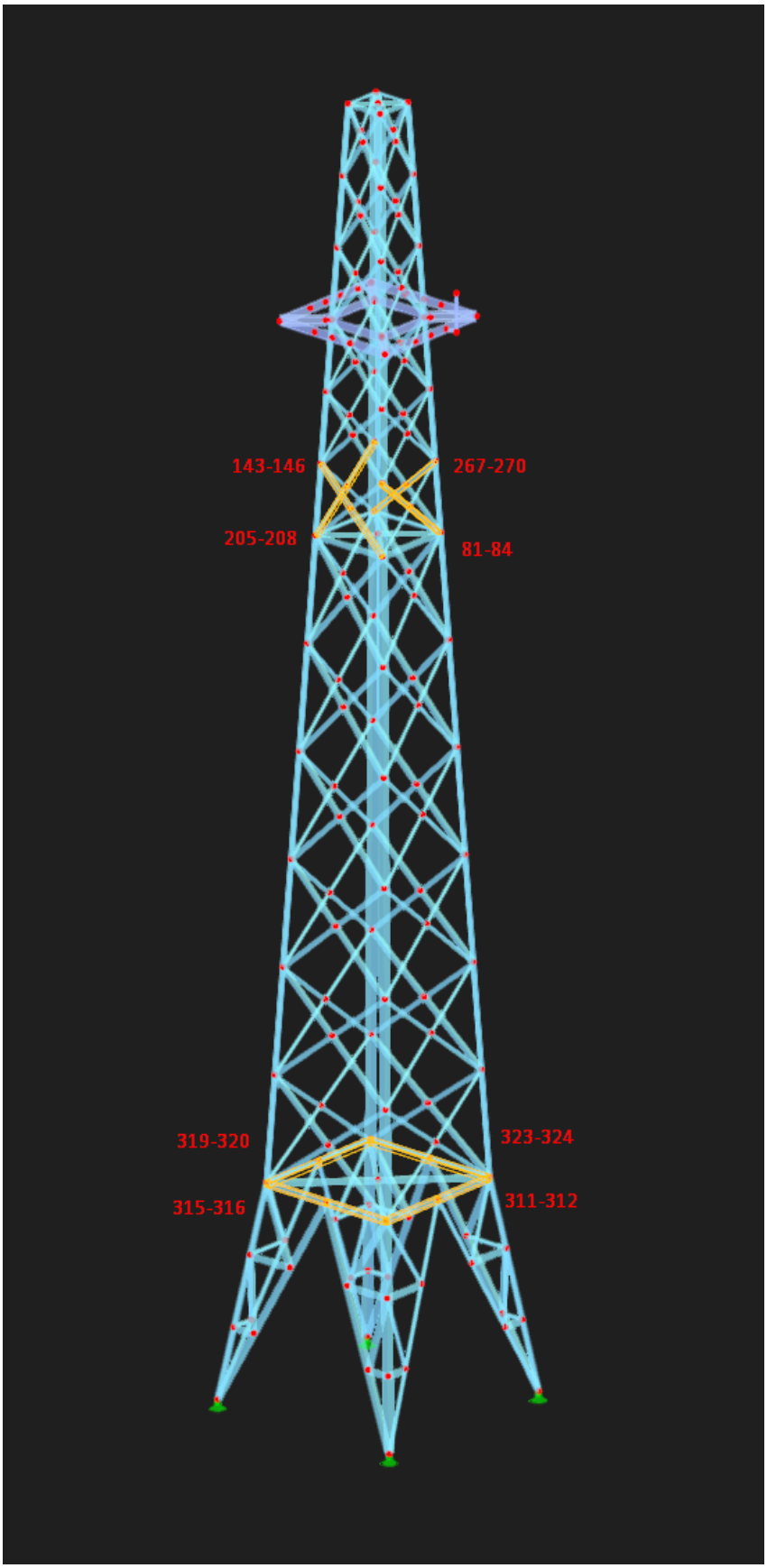
143-146
267-270
205-208
81-84
319-320
323-324
315-316
311-312

As shown by the previous figure, the elements that present the highest stress ratio can be collected in two sets. As it could be expected there is only partial correspondence between the critical cross sections obtained from Response Spectrum Analysis and the Time History Analysis. It is first interesting to point out that the RSA results are completely symmetric whereas the THA are not. This is consistent with the spectra in the x and y direction being equal as prescribed by EN1998-1 in the RSA, as opposed to the recorded accelerogram considered for the THA. Even if the input spectra differ significantly, elements 311-312 appear as critical sections in both analysis. This is not surprising as those members are at the interface between the basal part and the upper part of the structure, which is where the load is transferred from the main truss structure to the support trusses. However it is apparent how the RSA produces significantly lower stress-ratios. Finally, the set of elements located in the upper part of the structure (81,84,143,146,205,208,267,270) do not find correspondence in the THA results. Relatively to the RSA results alone, this is explained by a higher relevance of horizontal excitations in the RSA. In relation to the THA, the dominance of vertical accelerations make these members irrelevant compared to others.

4.3 Part C

An incremental number of modes was considered in order to obtain a 90% cumulative sum of modal participation factors, as recommended by EN1998-1.

N Modes	X	Y	Z	ϕ_x	ϕ_y	ϕ_z
10	52.44 %	52.40 %	0.28 %	61.85 %	61.86 %	5.69 %
50	72.97 %	73.01 %	2.26 %	70.04 %	70.02 %	43.17 %
100	96.24 %	96.31 %	46.66 %	92.35 %	92.24 %	83.58 %
500	98.01 %	98.01 %	79.69 %	96.39 %	96.40 %	93.43 %

The Response Spectrum Analysis was carried out with a 500 mode approximation. It is worth noting that the summation of mass ratios in the Z direction does not meet the recommended value. The main reason behind such truncation decision was ensuring computational manageability of the model. From a physical point of view, this modelling choice should not impact significantly the results of the analysis, since the (cantilever) beam-like behavior of the structure should guarantee high resistance in the axial direction. Moreover, the dominant excitations imposed by EN1998-1 are horizontally directed, which further supports the implemented assumption, however this vulnerability should not go overlooked when vertical accelerations are relevant, as shown by the results of Time History Analysis where mode 41 proved to be determining.

Elaborating further on the sensitivity of the results to the number of modes used in the analysis, it can be observed by comparing the previous and the following table that no difference is encountered in the numerical results between 50, 100 and 500 (disclaimer: Member 115 is a symmetric counterpart of Member 239). A small numerical difference is instead recorded between 10 and 50 modes approximation.

N Modes	Max Disp. X	Max Disp. Y	Max Disp. Z	Max Disp. ϕ_x	Max Disp. ϕ_y	Max Disp. ϕ_z
10	61.4 mm	70.1 mm	11.5 mm	25.5 mrad	11.9 mrad	36.4 mrad
	Member	Member	Member	Member	Member	Member
	No. 313	No. 365	No. 365	No. 365	No. 301	No. 119
50	61.3 mm	61.3 mm	11.5 mm	12.0 mrad	12.0 mrad	36.5 mrad
	Member	Member	Member	Member	Member	Member
	No. 313	No. 309	No. 333	No. 115	No. 177	No. 181
100	61.3 mm	61.3 mm	11.5 mm	12.0 mrad	12.0 mrad	36.5 mrad
	Member	Member	Member	Member	Member	Member
	No. 313	No. 309	No. 333	No. 239	No. 177	No. 181
500	61.3 mm	61.3 mm	11.5 mm	12.0 mrad	12.0 mrad	36.5 mrad
	Member	Member	Member	Member	Member	Member
	No. 313	No. 309	No. 333	No. 239	No. 177	No. 181

4.4 Part D

The structure is able to withstand the standardized seismic loads prescribed by EN1998-1. The computed stress ratios are well within unity check for all members. Additionally, no significant resonance was found.

5 Section 6 - Soil Structure Interaction

A preliminary design of the foundation was carried out as a first step. In order to match the double symmetry of the structure a square slab was the preferred choice. The dimensions were derived based on the maximum overturning moment developed during the pushover analysis, corresponding to 2811 kNm. Within the scope of approximation, a linear stress distribution was assumed along the length (maximum soil stress il reached on the left side and no lift was considered on the right side) and such distribution was assumed to be constant along width. An arbitrary depth of 0.3 m was consider a valid first guess based on a similar example in the study material.

Equilibrium: $M_{pushover} = (\frac{c_u L}{2} \cdot L) \cdot \frac{L}{6}$

Dimensions: $L = B = \sqrt[3]{\frac{12 * M_{pushover}}{c_u}} = 8.77m$

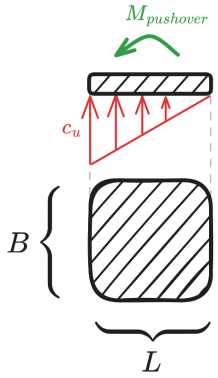

5.1 Part A - Frequency Dependent Soil Stiffness Matrix

[3]:
```
# Soil Properties (indipendent of Student Number)
nu = 0.33       #[-] Poisson Ratio
c_u = 50e3      #[Pa] Undrained Shear Strength
v_s = 160       #[m/s] Velocity of shear waves in soil
rho = 1800      #[kg/m^3] Soil Density
beta = 0.05     #[-] Soil hysteretic (material) damping (arbitrarily chosen)

# Foundation dimensions (rectangular slab shallow foundation)
side_x = side_y = 8.77 #[m] As a first implementation the slab is as large as␣
 ↪the base of the tower
depth = 0.3 #[m] height of foundation

# Structure
## Modal parameters from RFEM model (mode 2)
omega = 23.047 #[rad/s] Frequency of interest (Mode 2 - Main mode in X direction)
```

The frequency dependent dynamic stiffness matrix was derived according to the model proposed for a surface foundation on a homogenous half space as per Gazetas, G. (1991).

- Citation: Gazetas, G. 1991. Formulas and charts for impedances of surface and embedded foundations. Journal of Geotechnical Engineering, 117(9), 1363–1381. https://doi.org/10.1061/(asce)0733-9410(1991)117:9(1363)

[4]:
```
L = side_x/2                                    #[m] Half-length between center of␣
 ↪the circumscribed rectangle and side X-direction (major direction)
B = side_y/2                                    #[m] Half-width between center of␣
 ↪the circumscribed rectangle and side Y-direction (minor direction)
A_b = side_x*side_y                             #[m] Foundation surface area
I_bx = side_x*side_y**3/12                      #[m^4] Area moment of inertia␣
 ↪about x-axis
I_by = side_x**3*side_y/12                      #[m^4] Area moment of inertia␣
 ↪about y-axis
I_bz = side_x*side_y*(side_x**2+side_y**2)/12 #[m^4] Area moment of inertia␣
 ↪about z-axis
G = c_u                                         #[Pa] Shear modulus
v_la = 3.4*v_s/(np.pi*(1-nu))                   #[m/s] Lymer's analog wave␣
 ↪velocity (formula from cited paper)
chi = A_b/(4*L**2)                              #[-] Parameter from cited␣
 ↪paper'"Part B - Notebook (Answers 3-6).ipynb"

print("\nINPUT RECAP:")
print(f"L: {L:.3e} m")
print(f"B: {B:.3e} m")
print(f"A_b: {A_b:.3e} m")
print(f"I_bx: {I_bx:.3e} m^4")
print(f"I_by: {I_by:.3e} m^4")
```

```
print(f"I_bz: {I_bz:.3e} m^4")
print(f"G: {G:.3e} Pa")
print(f"v_la: {v_la:.3e} m/s")
print(f"chi: {chi:.3e} -")

#Static Stiffness
K_z = (2*G*L/(1-nu))*(0.73+1.54*chi**0.75)
K_y = (2*G*L/(2-nu))*(2+2.50*chi**0.85)
K_x = K_y - (0.2/(0.75-nu))*G*L*(1-(B/L))
K_rx = (G/(1-nu))*I_bx**0.75*(L/B)**0.25*(2.4+0.5*(B/L))
K_ry = (3*G/(1-nu))*I_by**0.75*(L/B)**0.15
K_t = 3.5*G*I_bz**0.75*(B/L)**0.4*(I_bz/B**4)**0.2


# Dynamic Stiffness
a_0 = omega * B / v_s
print(f"a_0: {a_0:.3e} ")

## Table values
k_z_tab = 0.92          #(table Fig.2(a))
k_y_tab = 0.94          #(table Fig.2(b))
k_x_tab = 1             #(constant)
k_rx_tab = 1-0.20*a_0   #(Table 1)
k_ry_tab = 1-0.26*a_0   #(Table 1)
k_t_tab = 1-0.14*a_0    #(Table 1)

## Coefficients
K_z_dyn = K_z*k_z_tab
K_y_dyn = K_y*k_y_tab
K_x_dyn = K_x*k_x_tab
K_rx_dyn = K_rx*k_rx_tab
K_ry_dyn = K_ry*k_ry_tab
K_t_dyn = K_t*k_t_tab

print("\nDynamic Stiffness Coefficients:")
print(f"K_z_dyn: {K_z_dyn:.3e} N/m")
print(f"K_y_dyn: {K_y_dyn:.3e} N/m")
print(f"K_x_dyn: {K_x_dyn:.3e} N/m")
print(f"K_rx_dyn: {K_rx_dyn:.3e} N/m")
print(f"K_ry_dyn: {K_ry_dyn:.3e} N/m")
print(f"K_t_dyn: {K_t_dyn:.3e} N/m")

#  Radiation Dashpot Coefficients
## Table values
c_z_tab = 0.93 #(table Fig.2(c))
c_y_tab = 0.87 #(table Fig.2(d))
c_rx_tab = 0.18 #(table Fig.2(e))
```

```
c_ry_tab = 0.18 #(table Fig.2(f))
c_t_tab = 0.15 #(table Fig.2(g))

## Coefficients
C_z = rho*v_la*A_b*c_z_tab
C_y = rho*v_s*A_b*c_y_tab
C_x = rho*v_s*A_b
C_rx = rho*v_la*I_bx*c_rx_tab
C_ry = rho*v_la*I_by*c_ry_tab
C_t = rho*v_s*I_bz*c_t_tab

## Total Damping (inclusive of materia damping)
C_z_tot = C_z+2*K_z_dyn*beta/omega
C_y_tot = C_y+2*K_y_dyn*beta/omega
C_x_tot = C_x+2*K_x_dyn*beta/omega
C_rx_tot = C_rx+2*K_rx_dyn*beta/omega
C_ry_tot = C_ry+2*K_ry_dyn*beta/omega
C_t_tot = C_t+2*K_t_dyn*beta/omega
print("\nTotal Damping Coefficients")
print(f"C_z_tot: {C_z_tot:.3e} N/(m*s)")
print(f"C_y_tot: {C_y_tot:.3e} N/(m*s)")
print(f"C_x_tot: {C_x_tot:.3e} N/(m*s)")
print(f"C_rx_tot: {C_rx_tot:.3e} N/(m*s)")
print(f"C_ry_tot: {C_ry_tot:.3e} N/(m*s)")
print(f"C_t_tot: {C_t_tot:.3e} N/(m*s)")

# Dynamic Stiffness Matrix (inclusive of damping)
K_dyn_vec_6dof = [ K_x_dyn, K_y_dyn, K_z_dyn, K_rx_dyn, K_ry_dyn, K_t_dyn ]
C_tot_vec_6dof = [ C_x_tot, C_y_tot, C_z_tot, C_rx_tot, C_ry_tot, C_t_tot ]
K_tilde_6dof = np.diag([k+1j*omega*c for k,c in␣
 ↪zip(K_dyn_vec_6dof,C_tot_vec_6dof)])
print("\nDynamic Stiffness Matrix (inclusive of damping):")
print(K_tilde_6dof)
```

```
INPUT RECAP:
L: 4.385e+00 m
B: 4.385e+00 m
A_b: 7.691e+01 m
I_bx: 4.930e+02 m^4
I_by: 4.930e+02 m^4
I_bz: 9.859e+02 m^4
G: 5.000e+04 Pa
v_la: 2.584e+02 m/s
chi: 1.000e+00 -
a_0: 6.316e-01

Dynamic Stiffness Coefficients:
```

```
K_z_dyn: 1.367e+06 N/m
K_y_dyn: 1.111e+06 N/m
K_x_dyn: 1.182e+06 N/m
K_rx_dyn: 1.978e+07 N/m
K_ry_dyn: 1.958e+07 N/m
K_t_dyn: 3.415e+07 N/m

Total Damping Coefficients
C_z_tot: 3.328e+07 N/(m*s)
C_y_tot: 1.928e+07 N/(m*s)
C_x_tot: 2.216e+07 N/(m*s)
C_rx_tot: 4.137e+07 N/(m*s)
C_ry_tot: 4.136e+07 N/(m*s)
C_t_tot: 4.274e+07 N/(m*s)

Dynamic Stiffness Matrix (inclusive of damping):
[[ 1181586.82634731+5.10630301e+08j        0.        +0.00000000e+00j
         0.        +0.00000000e+00j        0.        +0.00000000e+00j
         0.        +0.00000000e+00j        0.        +0.00000000e+00j]
 [       0.        +0.00000000e+00j  1110691.61676647+4.44256633e+08j
         0.        +0.00000000e+00j        0.        +0.00000000e+00j
         0.        +0.00000000e+00j        0.        +0.00000000e+00j]
 [       0.        +0.00000000e+00j        0.        +0.00000000e+00j
   1366811.04477612+7.67044678e+08j        0.        +0.00000000e+00j
         0.        +0.00000000e+00j        0.        +0.00000000e+00j]
 [       0.        +0.00000000e+00j        0.        +0.00000000e+00j
         0.        +0.00000000e+00j 19781320.21990046+9.53351004e+08j
         0.        +0.00000000e+00j        0.        +0.00000000e+00j]
 [       0.        +0.00000000e+00j        0.        +0.00000000e+00j
         0.        +0.00000000e+00j        0.        +0.00000000e+00j
  19575778.96330155+9.53330450e+08j        0.        +0.00000000e+00j]
 [       0.        +0.00000000e+00j        0.        +0.00000000e+00j
         0.        +0.00000000e+00j        0.        +0.00000000e+00j
         0.        +0.00000000e+00j 34151351.57732812+9.85039369e+08j]]
```

The foundation-soil interaction was simulated using four discrete nodal supports positioned at the corners of the foundation . The soil spring constants, derived from Gazetas tables were distributed among these four corner nodes to accurately capture the load transfer mechanism and soil response under various loading conditions.The damping dashpots were neglected as a conservative assumption.

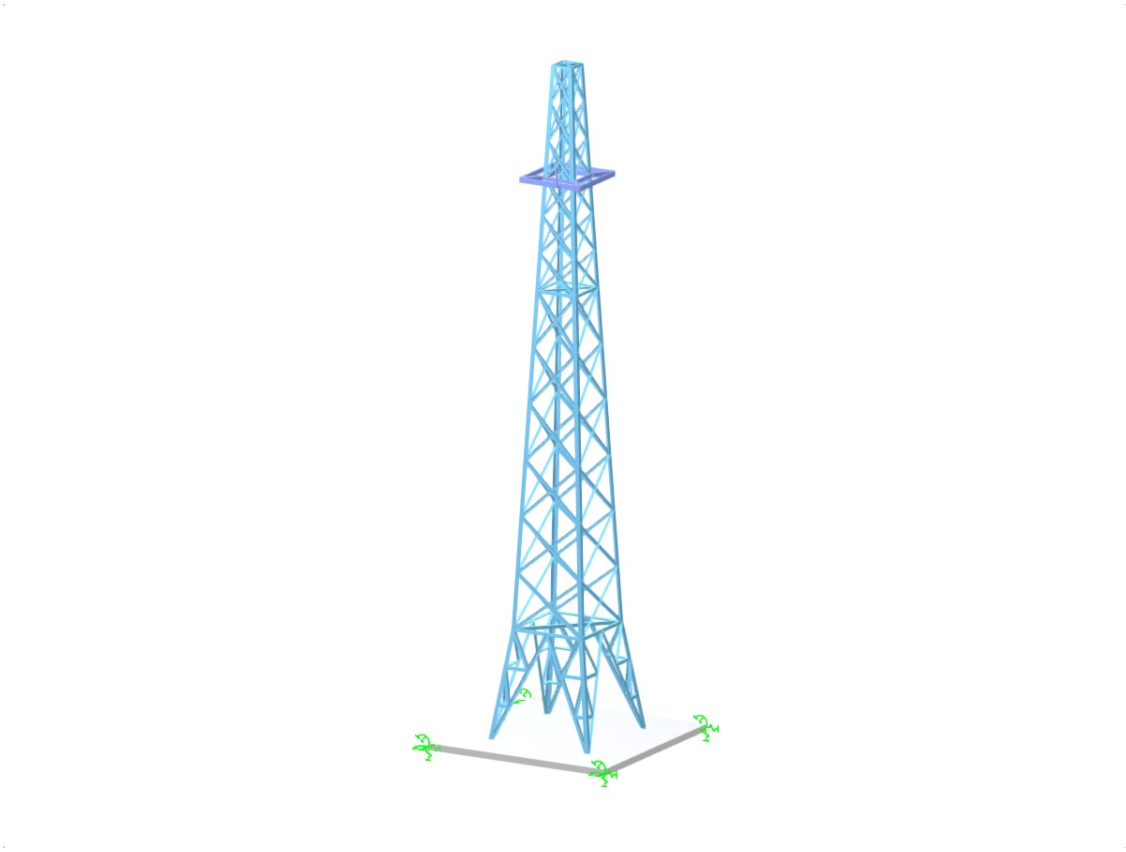

Response spectrum analysis was conducted to evaluate the structural behavior under dynamic loading conditions. The summary of displacements obtained from this analysis is presented below.

Description	Value	Unit	Notes
Maximum displacement in X-direction	653.5 mm	mm	Member No. 313, x: 0.457 m
Maximum displacement in Y-direction	664.1 mm	mm	Member No. 309, x: 0.457 m
Maximum displacement in Z-direction	229.5 mm	mm	FE node No. 177: (-4.387, 4.387, 30.000 m)
Maximum vectorial displacement	951.7 mm	mm	Member No. 1, x: 0.000 m
Maximum rotation about X-axis	24.6 mrad	mrad	Member No. 365, x: 0.112 m
Maximum rotation about Y-axis	23.7 mrad	mrad	Member No. 150, x: 1.713 m
Maximum rotation about Z-axis	4.5 mrad	mrad	Member No. 119, x: 0.569 m

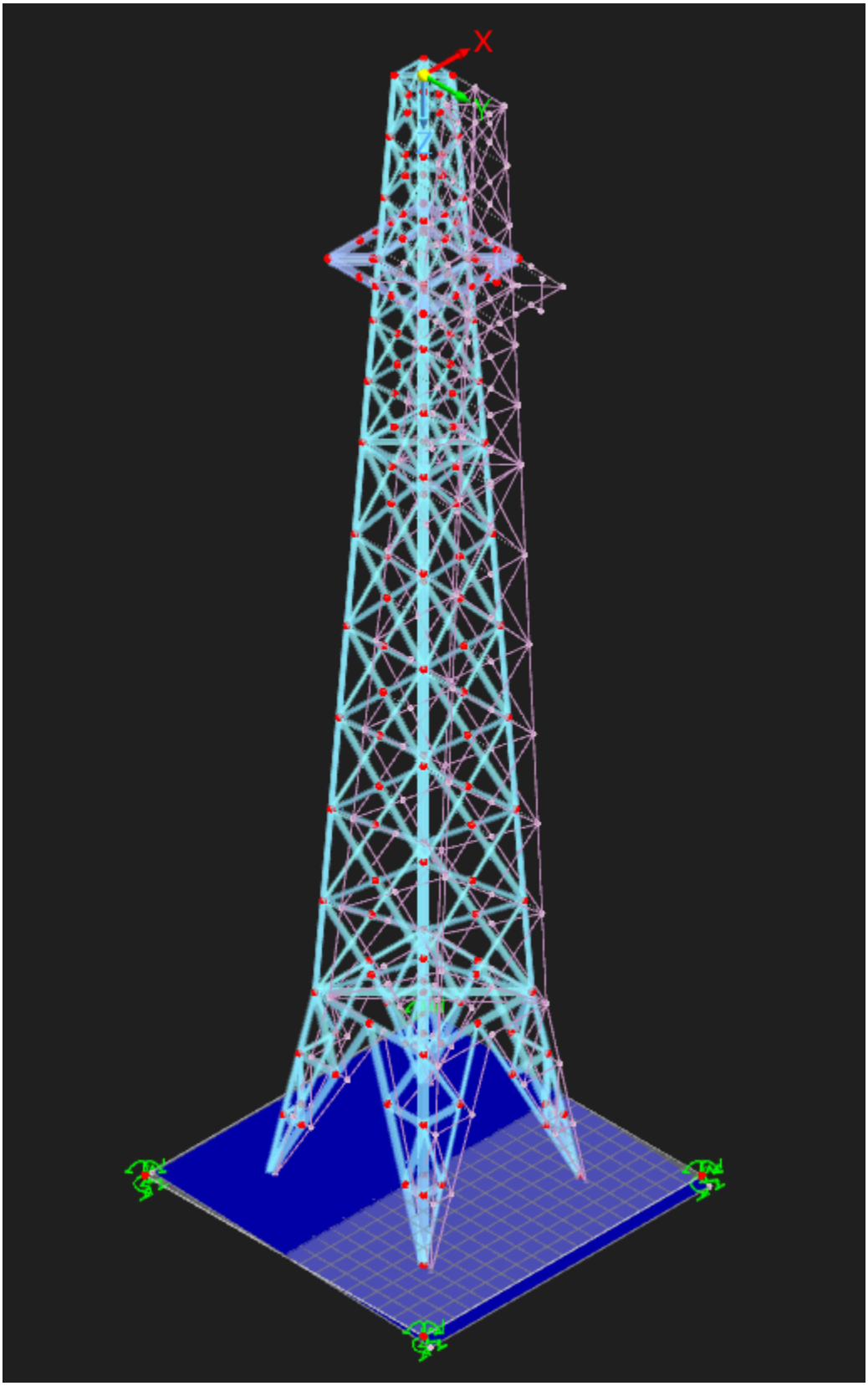

Modal Shape 1

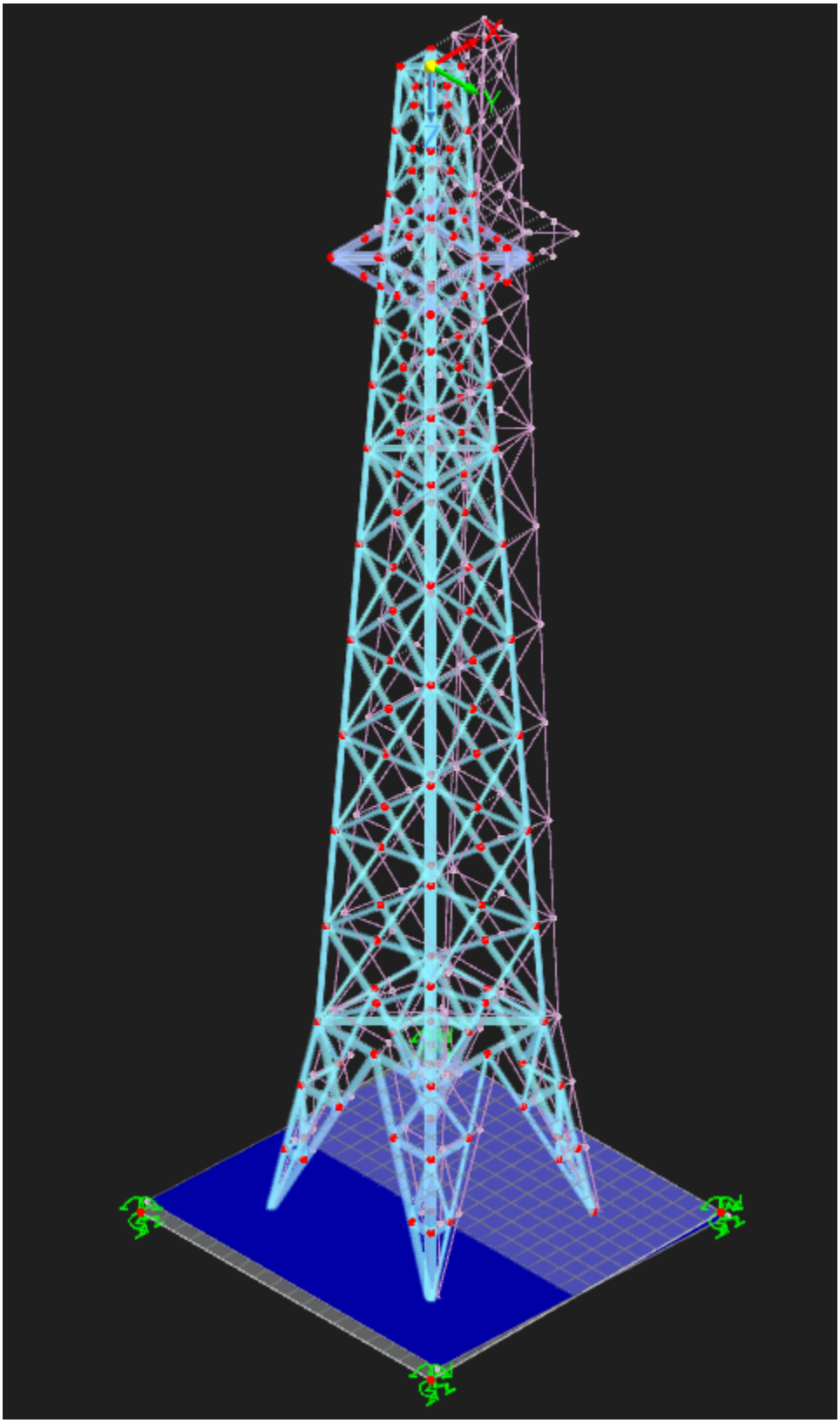

Modal Shape 2

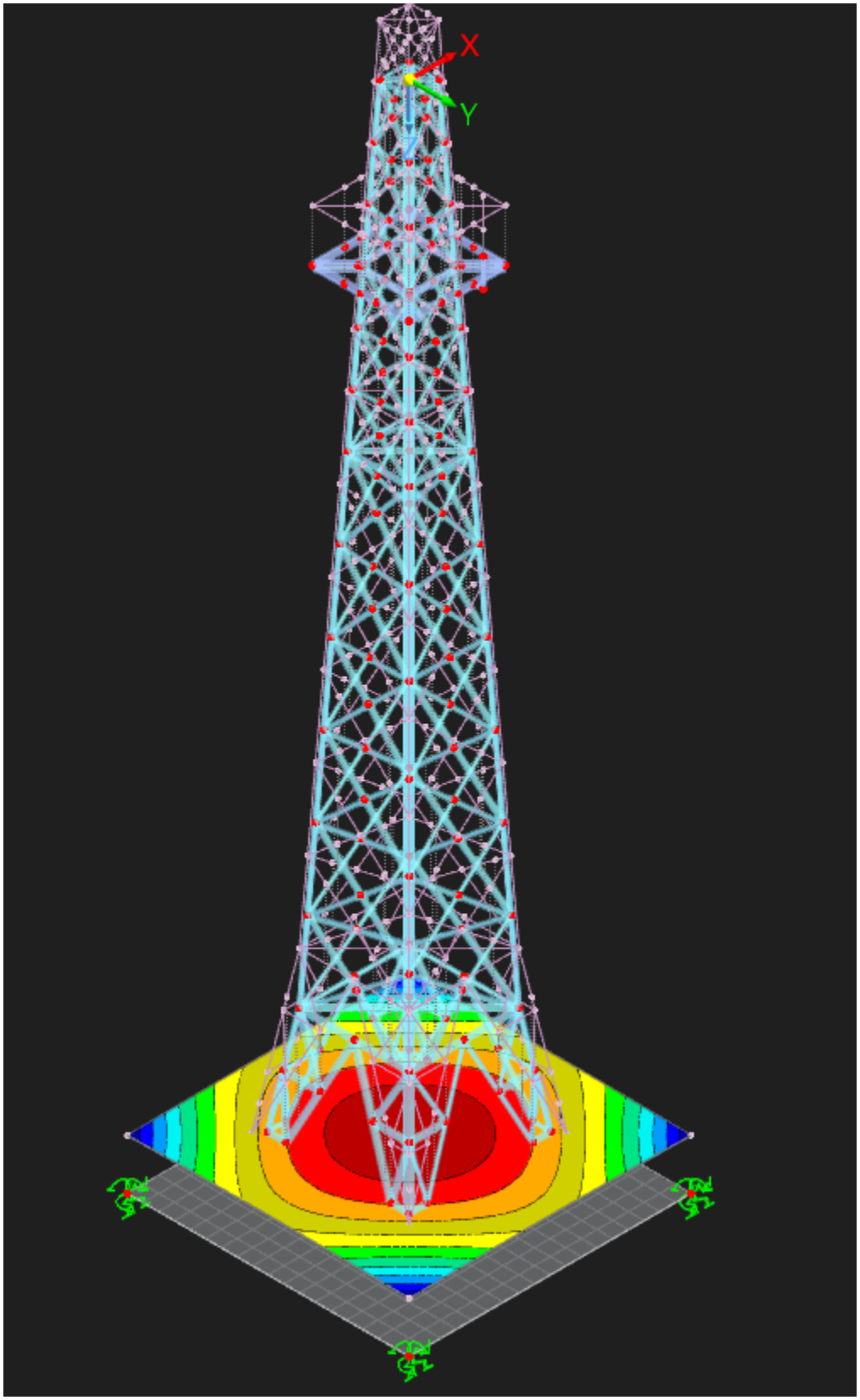

Modal Shape 3

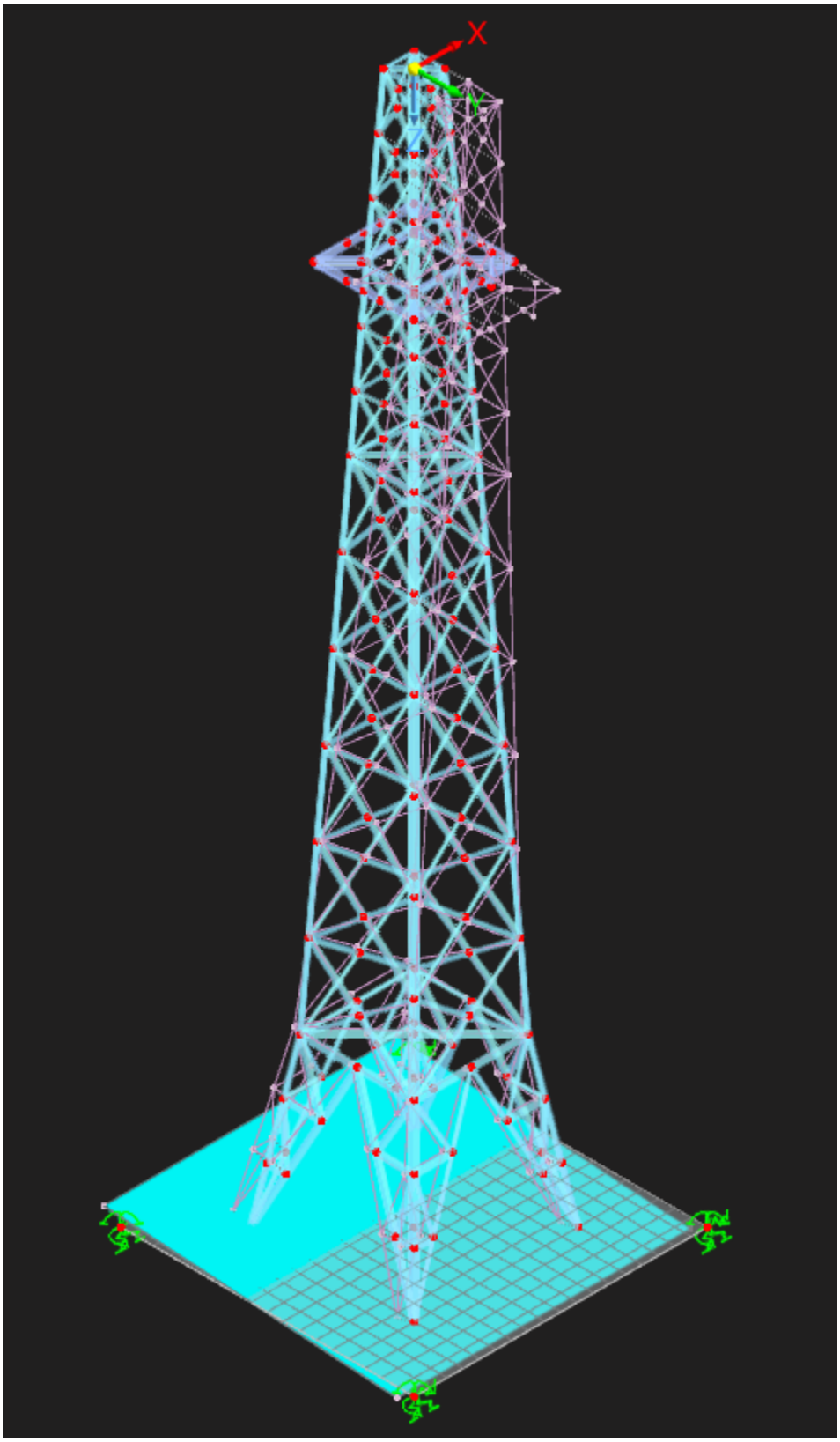

Modal Shape 4

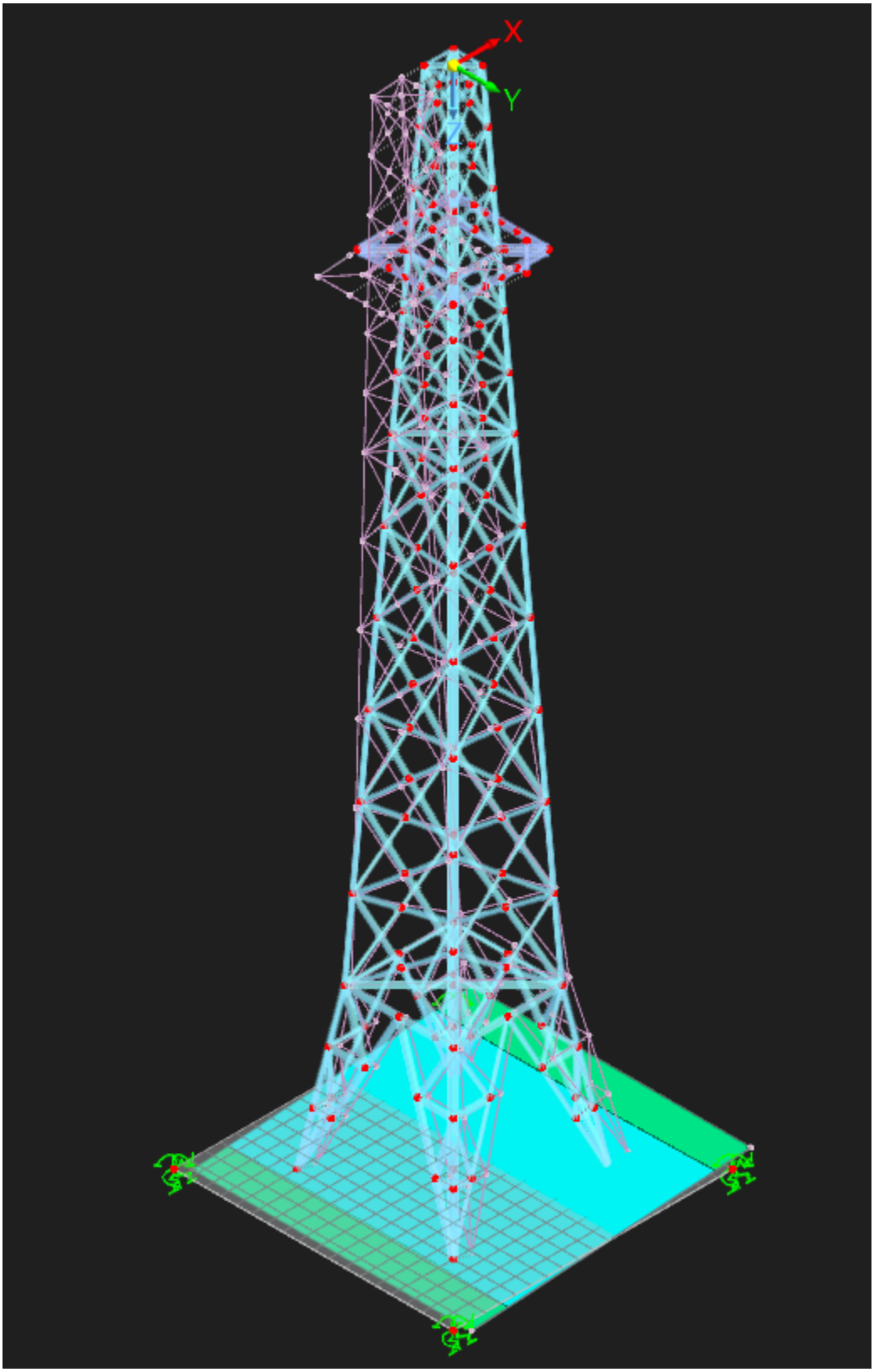

Modal Shape 5

Implementing SSI yields period lengthening that shifts the tower's natural frequencies to lower values.The distinct modes observed in each analysis case highlight how foundation and soil properties significantly alter the load transfer mechanisms from the superstructure to the ground resulting in non-uniform stress distributions that would not be captured in a fixed-base analysis. The first two modes are mostly translational whereas we can see third mode capturing significant vertical deformations. Mode shapes and modal participation factors become redistributed, with translational and torsional modes coupling more strongly, thereby affecting the accuracy of modal combination methods in RSA. The RSA results with the elastic foundation springs demonstrate a significant increase in maximum structural displacements compared to the fixed-support analysis presented earlier.Additionally, since the damping contribution of soil is neglected, this could further contribute to the higher observed responses.The higher displacements observed in the tabulated results reflect the more realistic structural behavior under seismic loading.These insights underscore the importance of incorporating SSI in RSA for telecommunication towers to capture realistic dynamic behavior and avoid under- or over-design based on rigid support assumptions.

5.2 Part B

As previously mentioned, mode 2 presents an Effective Modal Mass factor of 0.45, it was therefore considered the most appropriate to describe the system in a Single Degree of Freedom simplified system. The mass and moment of inertia of the SDoF system correspond to the effective modal mass in the translational x direction and rotational effective mass about the y-axis of the MDoF model. Both parameters can be extracted from the finite element model assembled in RFEM. The modal height can be computed as $h^* = \frac{\Gamma_{ry}}{\Gamma_t}$. A modal damping ratio of $\zeta^* = 0.048$ is assumed, therefore $c^* = 2\zeta^* m^* \omega$. Finally the modal stiffness can be derived as $k^* = \omega^2 M^*$

A summary of the properties used in the conversion from MDoF to SDoF is presented in the following table:

Parameter	Value	Origin
Modal mass	1683 kg	RFEM
Effective Modal Mass (x) > m	3940 kg	RFEM
Effective Modal Mass (r-y) > J	371117 $kg \cdot m^2$	RFEM
Γ_t	2575	RFEM
Γ_{ry}	24995	RFEM
h^*	9.705 m	Computed
c^*	3724 $kg \cdot rad/s$	Computed
k^*	2092787 $kg \cdot rad^2/s^2$	Computed

Taking into account the presence of the soil the SDOF system can therefore be represented as follows.

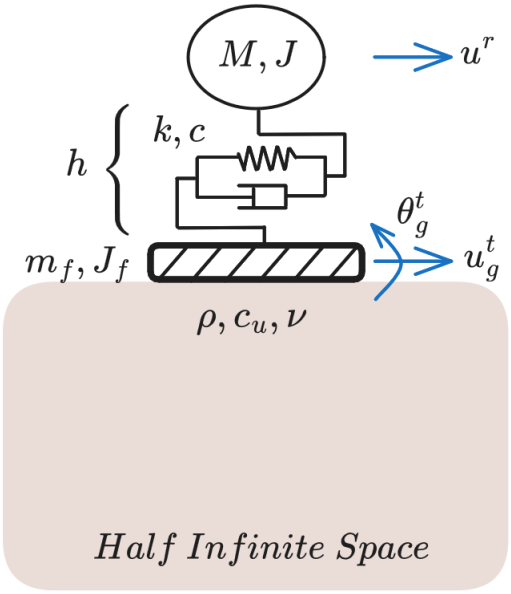

Where:

$u^r(t)$ relative displacement between top mass and foundation

$u_g^t(t) = u_g(t) + u_g^I(t)$ with: $u_g^t(t)$ total ground displacement, $u_g(t)$ free-field ground displacement, $u_g^I(t)$ ground displacement deriving from soil-structure interaction

$\theta_g^t(t) = \cancel{\theta_g(t)} + \theta_g^I(t)$ with $\theta_g^t(t)$ total rocking motion of the ground, $\theta_g(t)$ free-field rocking motion (neglected), $\theta_g^I(t)$ rocking motion due to soil-structure interaction

The system can then be divided in two subsystems in order to analyze the interaction between soil and structure.

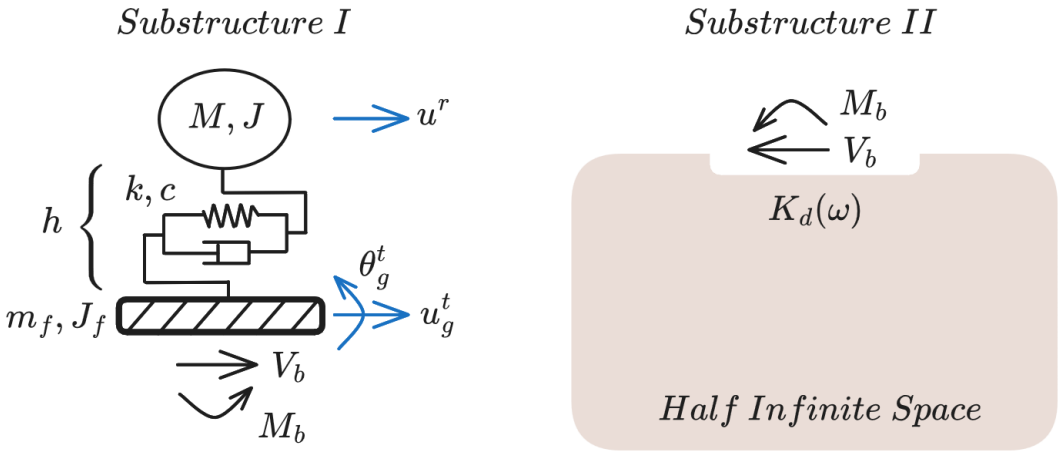

The translational equilibrium equation for the top mass can be formulated as:

$m\ddot{u^r}(t) + c\dot{u^r}(t) + ku^r(t) + m(\ddot{u}_g(t) + \ddot{u}_g^I(t) + h\ddot{\theta}_g^I(t)) = 0$

The translational equilibrium at soil-structure interface can be formulated as:

$m(\ddot{u}_g(t) + \ddot{u}_g^I(t) + \ddot{u^r}(t) + h\ddot{\theta}_g^I(t)) + m_f(\ddot{u}_g(t) + \ddot{u}_g^l(t)) = V_b(t)$

The rotational equilibrium at the soil-structure interface can be formulated as:

$mh(\ddot{u}_g(t) + \ddot{u}_g^l(t) + \ddot{u^r}(t)) + (mh^2 + J + J_f)\ddot{\theta}_g^l(t) = M_b(t)$

Using a Fourier Transform the system can be converted to the frequency domain as follows:

$(-\omega^2 m + i\omega c + k)\tilde{u^r}(\omega) - \omega^2 m\tilde{u}_g^I(\omega) - \omega^2 mh\tilde{\theta}_g^I(\omega) = -m\tilde{a_g}(\omega)$

$-\omega^2 m\tilde{u^r}(\omega) - \omega^2(m + m_f)\tilde{u}_g^I(\omega) - \omega^2 mh\tilde{\theta}_g^I(\omega) - \tilde{V}_b(\omega) = -(m + m_f)\tilde{a}_g(\omega)$

$-\omega^2 mh\tilde{u^r}(\omega) - \omega^2 mh\tilde{u}_g^I(\omega) - \omega^2(mh^2 + J + J_f)\tilde{\theta}_g^I(\omega) - \tilde{M}_b(\omega) = -mh\tilde{a}_g(\omega)$

Where: $\tilde{a_g} = \tilde{i\ddot{u}_g}$

Moreover $\tilde{V}_b(\omega)^{SS-I} = -\tilde{V}_b(\omega)^{SS-II}$ and $\tilde{M}_b(\omega)^{SS-I} = -\tilde{M}_b(\omega)^{SS-II}$

$\tilde{V}_b(\omega)$ and $\tilde{M}_b(\omega)$ can therefore be derived from the soil stiffness matrix as:

$\tilde{V}_b(\omega) = -\tilde{k}_{xx}(\omega)\tilde{u}_g^I(\omega) - \cancel{\tilde{k}_{x\theta}(\omega)\tilde{\theta}_g^I(\omega)} - i\omega\tilde{c}_{xx}(\omega)\tilde{u}_g^I(\omega) - \cancel{i\omega\tilde{c}_{x\theta}(\omega)\tilde{\theta}_g^I(\omega)}$

$\tilde{M}_b(\omega) = -\cancel{\tilde{k}_{\theta x}(\omega)\tilde{u}_g^I(\omega)} - \tilde{k}_{\theta\theta}(\omega)\tilde{\theta}_g^I(\omega) - \cancel{i\omega\tilde{c}_{\theta x}(\omega)\tilde{u}_g^I(\omega)} - i\omega\tilde{c}_{\theta\theta}(\omega)\tilde{\theta}_g^I(\omega)$

Soil stiffness coefficients were derived following the methodology presented in Gazetas, G. (1991). Formulas and charts for impedances of surface and embedded foundations. Journal of Geotechnical Engineering, 117(9), 1363–1381. (see part A). It is worth underlying that cross-coupling terms (translation-rotation interaction) can be neglected when dealing with shallow foundations.

After the final substitution, the system can therefore be rewritten in the following form:

$(-\omega^2 m + i\omega c + k)\tilde{u^r}(\omega) - \omega^2 m\tilde{u}_g^I(\omega) - \omega^2 mh\tilde{\theta}_g^I(\omega) = -m\tilde{a}_g(\omega)$

$-\omega^2 m\tilde{u^r}(\omega) + (\tilde{k}_{xx}(\omega) + i\omega\tilde{c}_{xx}(\omega) - \omega^2(m + m_f))\tilde{u}_g^I(\omega) - \omega^2 mh\tilde{\theta}_g^I(\omega) = -(m + m_f)\tilde{a}_g(\omega)$

$-\omega^2 mh\tilde{u^r}(\omega) - \omega^2 mh\tilde{u}_g^I(\omega) + (\tilde{k}_{\theta\theta}(\omega) + i\omega\tilde{c}_{\theta\theta}(\omega) - \omega^2(mh^2 + J + J_f))\tilde{\theta}_g^I(\omega) = -mh\tilde{a}_g(\omega)$

The algebraic system of equations can be solved for the three unknowns: $\tilde{u^r}(\omega)$, $\tilde{u}_g^I(\omega)$, $\tilde{\theta}_g^I(\omega)$

By adopting an analogous approach the system without soil structure interaction could be described by the following equations:

Equation of motion: $m\ddot{u^r}(t) + c\dot{u^r}(t) + ku^r(t) = -ma_g - \cancel{mh\theta_g}$

Equation of motion in frequency domain $(-\omega^2 m + i\omega c + k)\tilde{u^r}(\omega) = -m\tilde{a}_g(\omega)$

[5]:
```
# SDOF Model
m_modal = 1683      #[kg] modal mass
M_x = 3940          #[kg] effective translational modal mass in the x direction
J_y = 371117        #[kg*m^2] effective rotational modal mass about the y-axis␣
↪(moment of inertia)
```

```
gamma_t = 2575.4   #[-] translational participation factor in the x direction
gamma_ry = 24995.1 #[-] rotation participation factor about the y-axis
zeta_star = 0.048  #[-] modal damping ratio (mode 2, arbitrarily assumed)
omega_s = 23.044   #[rad/s] natural frequency of the SDoF model (mode 2)

h_star = gamma_ry/gamma_t
c_star = 2*zeta_star*m_modal*omega_s
k_star = omega_s**2*M_x

rho_f = 2400 #[kg/m^3] Density of concrete (arbitrarily chosen)
m_f = rho_f*side_x*side_y*depth #[kg] Mass of foundation
J_y_f = m_f*(side_x**2+depth**2)/12 #[kg*m^2] Moment of Inertia of foundation␣
 ↪about the y-axis

print("Parameter Recap:")
print(f"h_star: {h_star:.3f} m")
print(f"c_star: {c_star:.3f} kg*rad/s")
print(f"k_star: {k_star:.3f} kg*rad^2/s^2")

omega_table_max = 2*v_s/B
omega_domain = np.linspace(0.001, omega_table_max,10000) #Based on curves␣
 ↪applicability (domain from tables)

# Fitting of curves in tables
## Only c_ry
points = [[0, 0.25, 0.5, 0.65, 1, 1.5, 2],[0, 0.05, 0.125, 0.2, 0.3, 0.45, 0.55]]
c_ry_curve = np.poly1d(np.polyfit(points[0], points[1], 5))

# Polynomial graph as sanity check
# plt.plot(omega_domain, c_ry_curve(omega_domain*B/v_s))
# plt.show()

frf_ur_tilde = []
frf_ug_tilde = []
frf_thetag_tilde = []

for counter,omega in enumerate(omega_domain):

    # Frequency Dependent Coefficients for Dynamic Stiffness and Damping of Soil
    # (same as previous code-cell but repeated inside the loop only for relevant␣
 ↪directions of motion, necessary to account for frequency dependency)
    a_0 = omega*B/v_s

    K_y_static = (2*G*L/(2-nu))*(2+2.50*chi**0.85) #y coefficient is required to␣
 ↪compute K_x_static
    K_x_static = K_y_static - (0.2/(0.75-nu))*G*L*(1-(B/L))
    K_x_dyn = K_x_static*1 #Formula from table
```

```
    K_ry_static = (3*G/(1-nu))*I_by**0.75*(L/B)**0.15
    K_ry_dyn = (1-0.26*a_0) * K_ry_static

    C_x = rho*v_s*A_b
    C_x_tot = C_x + 2*K_x_dyn*beta/omega
    C_ry = rho*v_la*I_by*c_ry_curve(a_0)
    C_ry_tot = C_ry + 2*K_ry_dyn*beta/omega

    # Acceleration
    a_g_tilde = 1 #[(m/s^2)/Hz] Acceleration in the frequency domain (taken as␣
 ↪unitary for FRF computation)

    K_tilde_system = np.zeros((3,3), dtype=complex)
    K_tilde_system[0, 0] = -omega**2*M_x + 1j*omega*c_star + k_star
    K_tilde_system[1, 1] = K_x_dyn + 1j*omega*C_x_tot - omega**2*(M_x+m_f)
    K_tilde_system[2, 2] = K_ry_dyn + 1j*omega*C_ry_tot -␣
 ↪omega**2*(M_x*h_star**2+J_y+J_y_f)
    K_tilde_system[0, 1] = K_tilde_system[1, 0] = -omega**2*M_x
    K_tilde_system[0, 2] = K_tilde_system[2, 0] = -omega**2*M_x*h_star
    K_tilde_system[1, 2] = K_tilde_system[2, 1] = - omega**2*M_x*h_star

    F_tilde = np.array([-M_x*a_g_tilde, -(M_x+m_f)*a_g_tilde,␣
 ↪-M_x*h_star*a_g_tilde])

    u_r_tilde_omega , ug_tilde_omega , u_thetag_tilde_omega  = np.linalg.
 ↪solve(K_tilde_system, F_tilde)
    frf_ur_tilde.append(u_r_tilde_omega)
    frf_ug_tilde.append(ug_tilde_omega)
    frf_thetag_tilde.append(u_thetag_tilde_omega)


# No-interaction SDOF response

frf_ur_tilde_no_SSI = [-M_x*a_g_tilde/(-omega**2*M_x+1j*c_star*omega+k_star) for␣
 ↪omega in omega_domain]

plt.semilogy(omega_domain, np.abs(frf_ur_tilde_no_SSI), label=r"$Structure\␣
 ↪(excluding\ SSI)$")
plt.semilogy(omega_domain, np.abs(frf_ur_tilde), label=r"$Structure\ (including\␣
 ↪SSI)$")
plt.semilogy(omega_domain, np.abs(frf_ug_tilde), label=r"$Foundation\␣
 ↪Translation$")
plt.semilogy(omega_domain, np.abs(frf_thetag_tilde), label=r"$Foundation\␣
 ↪Rotation$")
plt.title("FRF Comparison between free-SDoF system and SSI")
plt.xlabel(r"$Frequency\ [rad/s]$")
```

```
plt.ylabel(r"$Motion\ [m/Hz]$")
plt.grid()
# plt.xlim(0, 10)
plt.legend()
```

```
Parameter Recap:
h_star: 9.705 m
c_star: 3723.173 kg*rad/s
k_star: 2092242.188 kg*rad^2/s^2
```

[5]: <matplotlib.legend.Legend at 0x25d5d88c440>

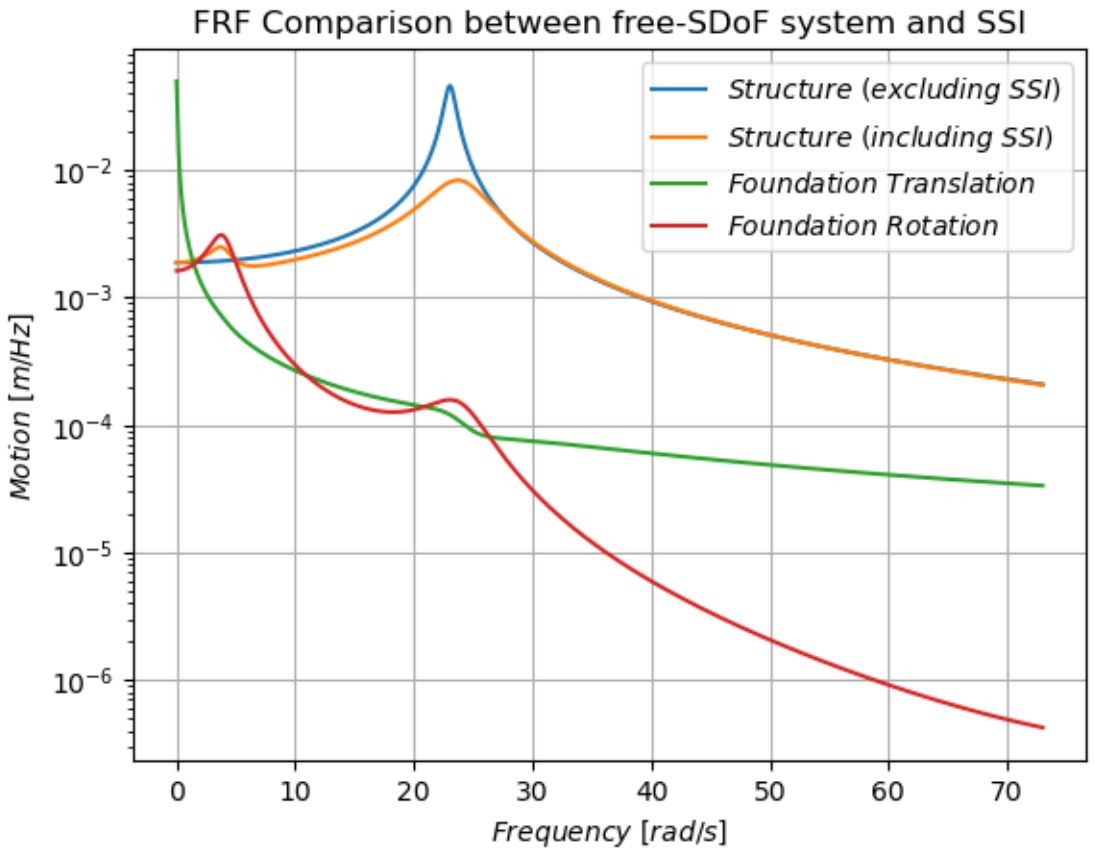

It is apparent how the introduction of the SSI has a significant impact on the dynamic response of the system. This is not only due to the soil behavior but also to the introduction of the foundation mass and the related degrees of freedom. The FRF of the structure inclusive of the interaction model shows a shifted and milder peak in the natural frequency corresponding to the vibration of the top mass. From the standpoint of the physical accuracy of the model, an important addition compared to the SDoF system without SSI is the energy dissipation due to soil material damping and radiation damping. Moreover a second peak appears in the structure response. Such peak is located at approximately 3 Hz and corresponds to the natural frequency of the rotational degree of freedom of the foundation.